WAVINESS OF THE SOUTHERN HEMISPHERE WINTERTIME POLAR AND SUBTROPICAL JETS

by

Jonathan E. Martin[1] and Taylor Norton[2]

[1]Department of Atmospheric and Oceanic Sciences
[2]Antarctic Meteorological Research Center
University of Wisconsin-Madison
Madison, WI 53706
USA

Corr. Author: Jonathan E. Martin, jemarti1@wisc.edu

ABSTRACT

The recently developed average latitudinal displacement (ALD) methodology is applied to assess the waviness of the austral winter subtropical and polar jets using three different reanalysis data sets. As in the wintertime Northern Hemisphere, both jets in the Southern Hemisphere have become systematically wavier over the time series and the waviness of each jet evolves quite independently of the other during most cold seasons. Also, like its Northern Hemisphere equivalent, the Southern Hemisphere polar jet exhibits no trend in speed (though it is notably slower) while its poleward shift is statistically significant. In contrast to its Northern Hemisphere counterpart, the austral subtropical jet has undergone both a systematic increase in speed as well as a statistically significant poleward migration. Composite differences between the waviest and least wavy seasons for each species suggest that the Southern Hemisphere's lower stratospheric polar vortex is negatively impacted by unusually wavy tropopause-level jets of either species. These results are considered in the context of trends in the Southern Annular Mode as well as the findings of other related studies.

KEYWORDS: Southern Hemisphere, winter, polar jet, subtropical jet, waviness

1. Introduction

Consideration of changes in the behavior of the tropopause-level jet streams in a warming world has been catalyzed by the construction of long-period reanalysis data sets over the past three decades (Kalnay et al, 1996; Kistler et al., 2001; Kobayashi et al. 2015; Copernicus Climate Change Services [CS3], 2017). Recent analyses employing these data sets (e.g. Archer and Caldiera, 2008; Barnes and Screen, 2015; Gallego et al. 2005; Manney and Hegglin, 2018; Peña-Ortiz et al. 2013; Vavrus et al. 2017), in tandem with a number of studies based upon climate model output (e.g. Barnes and Polvani, 2013; Lorenz and DeWeaver, 2007; Miller et al. 2006; Yin, 2005), have produced a consensus view that poleward displacement of both jets accompanies warming. Along with an interest in latitudinal position, nearly all of the aforementioned studies have also addressed either observed and/or forecasted changes in the speed of the jet streams.

In a recent paper Martin (2021) offered a feature-based analysis of the *waviness* of the tropopause-level polar and subtropical jets during Northern Hemisphere winter (DJF). The analysis proceeded from the results of Christenson et al. (2017) that identified the isentropic layers that house the two species of jets during NH winter. He found that 1) the polar jet (POLJ) has undergone a statistically significant poleward migration over the time series, not matched by the subtropical jet (STJ), and 2) neither jet species exhibited a trend in its speed. Additionally, the analysis showed that both jets have become systematically wavier over the last 6 decades.

By virtue of its land/sea distribution, enhanced lower tropospheric warming at high latitudes of the NH, known as Arctic amplification, has recently emerged as a prominent signal of climate change (e.g., Serreze et al. 2009; Screen and Simmonds, 2013: and references therein). Francis and Vavrus (2012) were among the first to propose that changes in the undulatory nature of the jet stream might be linked to Arctic amplification. This suggestion initiated a decade-long debate on this issue (e.g. Barnes, 2013; Blackport and Screen, 2020; DiCapua and Coumou, 2016; Francis, 2017; Francis and Vavrus, 2015; Francis et al. 2018; Martineau et al. 2017, Screen and Simmonds, 2013; Vavrus, 2018). As noted by Martin (2021), at least some of the controversy and attendant lack of consensus surrounding this question (Barnes and Polvani, 2015) was nourished by the absence of a robust method of assessing the waviness of the tropopause-level jets. The average latitudinal displacement (ALD) methodology introduced in Martin (2021) (briefly described later) offers one possible remedy to this deficiency.

The principle mode of variability in the SH extratropical circulation is the Southern Annular Mode (SAM, Limpasuvan and Hartmann, 1999; Gong and Wang, 1999; Thompson and Wallace, 2000), a nearly zonally symmetric structure with coincident geopotential height anomalies of opposite signs in Antractica and the middle latitudes. In the decades prior to 2000, the SH jets have shifted poleward and the SAM has tended toward positive polarity (e.g. Fogt and Marshall, 2020). These coincident trends have been presumed to be a result of ozone depletion. As the ozone recovers in the SH, simulations suggest a reversal of this trend may be forthcoming (WMO, 2022). Spenberger et al. (2020) have questioned whether the associated jet displacement also explains shifts in the storm tracks across the hemisphere. Instead they suggest that SAM can be interpreted as a measure of the degree of coupling (or decoupling) between Antractica and the southern mid-latitudes.

Recently, considerable attention has been devoted to interrogating the zonally asymmetric component of SAM (e.g. Fan 2007; Silvestri and Vera, 2009; Fogt et al. 2012; Rosso et al. 2018; Campetelli et al. 2022). This asymmetric component is characterized by a wave-3 pattern (Goyal et al., 2021; Goyal et al., 2022; Campetelli et al. 2022) with maximum amplitude at 250 hPa in the Pacific and may be determinative of the overall positive trend in the SAM over the reanalysis era. Such a wave-3, tropopause-level signal is immediately suggestive of the influence of the jets. These observations motivate consideration of direct measurement of the waviness of the SH wintertime jets.

Despite a number of recent studies that consider aspects of the interannual variability of the austral winter subtropical jet (e.g. Gillett et al., 2021; Maher et al. 2019), to our knowledge, a study by Gallego et al. (2005) is the only one to consider direct measurement of the waviness of the austral winter jets. They employed an objective method focused on identifying the geostrophic streamline of maximum average velocity at 200 hPa (i.e. the jet core at that level) to separately consider the behaviors of the STJ and POLJ. This method allowed consideration of the jets as continuous features around the hemisphere and thus enabled a number of novel analyses of their behavior and trends. With particular relevance to the present study, they considered a zonal index computed as the difference between the maximum and minimum latitude of the jet core (i.e. the streamline at the core of the jet) on each day. A similar metric, termed DayMaxMin, was employed by Barnes (2013) in her consideration of the behavior of the NH 500 hPa flow. Though insightful, such a metric does not comprehensively account for the waviness created by the full collection of troughs and ridges around the hemisphere that routinely characterizes the jets.

In this paper we apply the methodology of Martin (2021) to assess recent trends in the waviness of the SH wintertime polar and subtropical jets. The method of identifying the austral winter polar and subtropical jet locations in isentropic space is described in Section 2 along with a description of the data sets used. Also included there is a short description of the method of assessing waviness introduced in Martin (2021). In Section 3, elements of the long-term trend and interannual variability of the waviness of the austral winter polar and subtropical jets are presented along with differences between composites of the waviest and least wavy seasons for each species. A summary and conclusions are offered in Section 4.

2. Data and Methodology

In the foregoing analysis, the zonal (*u*) and meridional (*v*) winds as well as temperature (*T*), at 6 h intervals from three different reanalysis data sets are employed. 72 austral winters (JJA) (1948-2019) of the National Centers for Environmental Prediction/National Center for Atmospheric Research (NCEP/NCAR) reanalysis, at 17 isobaric levels to 10 hPa on a 2.5° latitude-longitude grid (Kalnay et al., 1996; Kistlet et al., 2001) are used. We employ 62 winters (1958-2019) of the Japanese 55-year (JRA-55) reanalysis with data on 60 vertical levels up to 0.1 hPa on a horizontal grid mesh of ~55 km (Kobayashi et al., 2015). Finally, the ERA5 reanalysis data set on 137 vertical levels from the surface to 80 km with a grid spacing of 31 km covering the period from 1979 to 2019 (Copernicus Climate Change Service [CS3], 2017) are used as well. The waviness of the jets is assessed in the context of understanding their relationships to the horizontal gradient of potential vorticity (PV) in prescribed isentropic layers. A similar approach was taken with respect to the STJ in recent work by Maher et al. (2019). The first step in the present analysis involves identification of the isentropic layers that house the austral winter jets. This was accomplished empirically by identifying the isentropic level at which the maximum wind speed was observed in each grid column (between 10 and 80°S) at each analysis time in JJA over the 62-year time series of the JRA-55 data set. The use of isentropic space here differs from the insightful approach taken by Manney et al. (2017) and Manney and Hegglin

(2018) which employed separate latitude and elevation criteria to differentiate between the STJ and the POLJ. Of the three data sets employed in the present work, the JRA-55 was chosen for this preliminary analysis step because both its length of time series as well as its horizontal and vertical resolutions are between those characterizing the other two data sets employed here. Following Koch et al. (2006) we only considered columns in which the integral average wind speed exceeded 30 ms^{-1} in the 100-400 hPa layer. The resulting distribution is clearly tri-modal with frequency maxima, and therefore separate jet features, approximately located in the 305-320, 340-355, and 395-410K isentropic layers (Fig. 1a). The latter isentropic layer appears in the lower stratosphere and is associated with the austral polar night jet (PNJ), which, being located *above* the tropopause, is not a focus of the present analysis. Further separation of the STJ and POLJ is achieved through reference to Fig. 2 of Gallego et al. (2005) which strongly implies that the STJ sharply peaks near 30°S while the POLJ more broadly peaks around 50°S. Accordingly, we further constrained the analysis to latitude bins 0-40°S for the STJ and 40 to 65°S for the POLJ. With this additional refinement, the analysis identifies the STJ in the 340-355K isentropic layer and the POLJ in the 310-325K isentropic layer (Fig. 1b). Similar analyses of the other two data sets (not shown) revealed the robustness of this result. It is important to note that 53.8% of all qualifying columns (to 380K) in the 0-40°S bin (STJ) were in the 340-355K layer while 46.8% of all qualifying columns in the 40-65°S bin (POLJ) were in the 310-325K layer supporting the isentropic assignments for the two species mentioned previously. It is immediately apparent, consistent with prior analyses (e.g. Bals-Elsholz et al. 2001, Nakamura and Shimpo 2004, Gallego et al. 2005), that the STJ is the dominant jet feature in the southern winter.

The analysis method to be used here involves assessment of the circulation which requires calculation of contour length. As a result, fair comparison among the different data sets requires adoption of a uniform grid spacing. Consequently, all three data sets were bilinearly interpolated onto isentropic surfaces at 5K intervals (from 280 to 380K) and 2.5° latitude-longitude grid spacing using programs within the General Meteorological Analysis Package (GEMPAK) (desJardins et al., 1991). The average PV and average zonal and meridional wind speeds in both the polar jet (310:325K) and subtropical jet (340:355K) layers were then calculated from the four times daily data for each day in each of the three time series.

As reviewed in Martin (2021), consideration of the quasi-geostrophic potential vorticity (QGPV), following Cunningham and Keyser (2004), demonstrates that local maxima in the cross-flow gradient of QGPV are collocated with maxima in the geostrophic wind speed. In the Southern Hemisphere, the jets lie on the high PV edge of this PV gradient. By searching through daily average isertels from -0.5 to -5.0 at 0.1 PVU intervals (1 PVU = 10^{-6} m^2 K kg^{-1} s^{-1}), the analysis identifies a "core isertel" along which the circulation per unit length (i.e. average speed) is maximized in the separate POLJ (310:325K) and STJ (340:355K) isentropic layers for every day in each of the time series. This core isertel is, by design, an analytical proxy for the jet core. A glimpse into the fidelity of this method in identifying the meandering cores of the POLJ and STJ jets is illustrated in Fig. 2. In each case the objectively identified core isertel, in black, lies very near, or at, the center of the analyzed isotach maxima around the hemisphere with physically defensible exceptions. For instance, the red dashed lines in Fig. 2b indicate portions of the bold black line in Fig. 2d (i.e. the overlying STJ core) suggesting that those portions of the isotach maxima in Fig. 2b that are somewhat removed from the POLJ core isertel are the lower portions of the overlying STJ core. Similarly, an extensive isotach maxima region in Fig. 2d has a blue dashed line, a portion of the bold black line in Fig. 2b, slicing through it. This region, well poleward of the STJ core isertel, is clearly the upper portion of the underlying POLJ core.

Figure 3a shows the average latitude for the core isertels of each jet species from each of the three reanalyses data sets used in the study. The analyses return essentially identical results for the core isertel of the STJ and very nearly identical results for the POLJ. Superimposing the NCEP-NCAR reanalysis' JJA average 200 hPa isotachs on top of the STJ core isertels (Fig. 3b) illustrates the fact that the average core isertel accurately represents the axis of the average STJ. The relationship is also strong between the POLJ core isertels and the 700 hPa average isotachs (Fig. 3c).

The waviness of each jet is assessed by calculating a hemispheric average of the meridional displacements of the core isertel from its equivalent latitude – the northern extent of a polar cap whose area is equal to the area enclosed by the core isertel. This metric is referred to as the average latitudinal displacement (ALD). The method does not require that the core isertel be the same in both jet layers on a given day, nor that it be the same from day-to-day in a given jet layer. Consequently, it is important to examine its distribution in each jet layer over the entire time series. Figure 4 portrays the frequency of occurrence of the core isertels in both the STJ and POLJ layers for each of the three time series. The STJ core isertels peak between -1.95 and -2.1 PVU across the three data sets. Considering all three data sets, 81.5% of all JJA days exhibit a core isertel between -1 and -3 PVU in the STJ layer. The POLJ distribution is shifted toward higher PV values. Overall, 74.8% of JJA days had a core isertel between -1 and -3 PVU in the POLJ layer. The frequency of occurrence in the several isertelic bins for each species of SH jet match quite well with what Martin (2021) found for the NH wintertime jets, even when accommodating for the different isentropic layer for the austral POLJ.

3. Analysis

The JJA seasonal average latitudinal displacement (ALD) of each jet is calculated as a 92-day average of the daily ALD in each cold season. The results are shown in Fig. 5. It is instantly clear that, as in the NH, the POLJ is wavier than the STJ and that both jets have become systematically wavier over the 62-year JRA-55 time series with $p < 0.004$ for both time series (a one-sided Student's *t*-test was employed). Interestingly, the austral winter STJ is less wavy than its NH counterpart but the waviness of both has increased identically at 0.005 deg/yr (0.0125 deg/yr for NCEP since 1958 and -0.001 deg/yr for ERA-5). The winter POLJ in the SH is, on the other hand, wavier than in the NH and is trending faster (0.017 versus 0.009 deg/yr; 0.023 deg/yr for NCEP since 1958 and 0.009 deg/yr for ERA-5) than its NH complement. Daily time series of the ALD of each jet can also be examined to determine the extent to which the waviness of the two jets covaries. Figure 6 illustrates the POLJ and STJ daily ALDs for 1999 from each of the three data sets. The low correlation between the waviness of the two species in this example year represents the rule rather than the exception. All told, more than 93% of the STJ and POLJ ALD seasonal time series constructed for this study are correlated with magnitudes less than 0.3. This result strongly suggests that the waviness of the two species evolves independently.

By definition, the average wind speed along the chosen core isertel on any given day represents the average jet speed for that species on that day. Time series of seasonal average jet core wind speeds for the wintertime STJ and POLJ in both hemispheres are shown in Fig. 7. As in the NH winter (Martin, 2021), the austral POLJ shows almost no trend in jet core speed and the slight change is not statistically significant. Notably, however, the SH POLJ is ~6 m s^{-1}

slower on average than its NH equivalent. Aside from the fact that the NCEP reanalysis is quite different from the JRA-55 until about 1970, the austral winter STJ exhibits a robust, and statistically significant (p-value < 0.001), increase in speed over the JRA-55 time series – in clear contrast to its NH counterpart. It is also apparent that the SH STJ is slightly weaker but less interannually variable than the NH STJ.

Another characteristic of interest that emerges directly from the ALD analysis method is the daily value of the jet core's equivalent latitude which closely approximates its zonally averaged position. Consequently, it is straightforward to construct a time series of the seasonal average equivalent latitudes of the two species of jets, shown in Fig. 8. Again, as in the NH, the poleward shift of the SH POLJ is occurring three times faster than that exhibited by the STJ. In contrast to the situation in the NH, however, the slight poleward displacement of the SH STJ ***is***, like that of the POLJ, statistically significant (p-values for the POLJ and STJ are <0.001 and 0.002, respectively). It is interesting to note that while the SH STJ is located at a roughly similar latitude as the NH STJ throughout the time series, the SH POLJ is ~4° further poleward during winter than the NH POLJ. Overall, a much more systematic and dramatic poleward migration of the two jets has occurred over the last 6 decades in SH winter as compared to NH winter.

Next we consider aspects of the analysis in the context of the SAM. Figure 9 shows a histogram of the JJA average SAM index (calculated after Gong and Wang (1999)) superimposed upon the average JJA ALD from the JRA-55 reanalysis. The tendency toward positive SAM over the time series appears to be reflected in the increase in ALD. However, the correlation between the two time series is 0.053 suggesting almost no relationship exists between the two.

In order to investigate the relationship of ALD to extremes in the polarity of the SAM index, the three winter months with the most positive and most negative SAM extremes since 1979 were considered. The core isertels of the POLJ (from the JRA-55 reanalysis) for each of these three months is portrayed in Fig. 10. Positive extremes of SAM (Figs. 10a, c, and e) show a clear poleward encroachment of the SH polar jet while negative extremes (Figs. 10b, d, and f) suggest the opposite. There appears to be no systematic connection, however, between extremes in SAM and the waviness of the POLJ as quantified by ALD.

Thus far the analysis has presented elements of the seasonal average behavior of the austral winter jet species. The methodology, of course, allows for evaluation of daily time series of ALD as well and, in fact, such an analysis underlies the presentation in Fig. 6. Using such daily time series, identification of the waviest and least wavy seasons for each jet species since 1979 is accomplished by summing the daily departures from calendar-day average ALD over the 92 days of each cold season. The list of such seasonally integrated departures from average waviness for each species of jet for each reanalysis data set is shown in Table 1. From this list, the 5 waviest and 5 least wavy seasons for each jet species were selected to construct composites of geopotential height at several isobaric levels employing the JRA-55 data. In the foregoing analysis, height differences are obtained by subtracting values associated with the composite least wavy seasons from those associated with the composite waviest seasons.

Figure 11a shows the 500 hPa geopotential height differences between the waviest and least wavy POLJ seasons. Wavy POLJ years are characterized by positive height anomalies over the continent and adjacent to its east and west coasts with belts of negative anomalies in a crescent stretching from southwest of Chile and then extending from the east coast of South America to southern Africa toward Australia, suggestive of a negative SAM. The strongest negative height anomalies in such seasons occur west of South Africa implying a slight weakening of the zonal winds just south of the Cape of Good Hope. Meanwhile wavy STJ years exhibit negative composite height differences in roughly the same locations as the positive composite differences just described for wavy POLJ years (Fig. 11b), suggestive of a positive SAM. These composite difference patterns strengthen slightly at 250 hPa (Fig. 12) suggesting an equivalent barotropic structure to the tropospheric portion of the difference fields.

The difference fields at 50 hPa imply that the waviness of both jets exerts an influence on the strength of the austral polar vortex in the lower stratosphere. The anomalous height field associated with wavy POLJ years (Fig. 13a) suggests a broad, though modest, anticyclonic circulation anomaly just off the pole in the Western Hemisphere. Such a perturbation flow would appear to interfere with the establishment and/or persistence of strong vortex flow in the same location. Wavy STJ seasons also impose a dipole of positive heights the axis of which stretches from Cape Horn to East Antarctica (Fig 13b). Such a configuration implies that the polar vortex is both weaker and displaced off the pole in winters with wavy STJs. Thus, the analysis suggests that in winters characterized by unusually wavy jets of either species, the SH polar vortex is likely weaker than normal. Further investigation of this intriguing implication is the subject of ongoing work.

4. Summary

The analysis presented here extends the application of a method developed by Martin (2021) to assess the waviness of the tropopause-level jets to analysis of the austral winter polar and subtropical jets. The analysis demonstrates that both jets have become systematically wavier over the past 60+ years. In addition, as in the NH, the waviness of the two species of austral winter jets is largely uncorrelated suggesting little systematic influence of one on the other throughout the season. Along with these similarities, there appear to be some fundamental asymmetries in the behavior of the wintertime tropopause-level jets between the hemispheres. The austral POLJ, like its NH counterpart, has exhibited no trend in its average speed over the time series, though it is notably slower than its NH wintertime equivalent. The STJ, on the other hand, has roughly the same speed as that in the NH winter but, unlike its NH counterpart, has undergone a systematic, statistically significant increase in its core speed since ~1960. Additionally, as opposed to the situation in the NH where only the POLJ migration toward to pole is statistically significant, ***both*** SH jets exhibit a significant poleward creep with the POLJ encroachment occurring at ~3x the rate of that characterizing the STJ.

The observed poleward migration of the STJ reported here is consistent with the analysis of CMIP5 simulations of historical and projected changes to the SH wintertime STJ by Chenoli et al. (2017). Though the present work employs a similarly dynamical definition of the STJ as that used in the study by Maher et al. (2019), they found no evidence of a poleward shift of the SH wintertime STJ. We suggest that the emphasis on empirically identifying a core isertel, rather than the maximum gradient of θ on a predetermined isertelic surface (i.e. 2 PVU as the dynamic tropopause) may account for this difference.

Finally, circulation differences between the waviest and least wavy POLJ and STJ seasons are manifest in both the troposphere and lower stratosphere. In the troposphere the signals are not as coherent in the SH as they were revealed to be in the NH (Martin 2021). Interestingly, the analysis implies that when either the POLJ or STJ is wavier than normal in a given winter, the lower stratospheric polar vortex is negatively impacted. Again, this is different from the behavior of the NH polar vortex in the face of extremes in waviness.

The results presented here, combined with those in Martin (2021), demonstrate that in both hemispheres a wavier than normal STJ during winter serves to weaken the lower stratospheric polar vortex. Though, as suggested by the analysis supporting Fig. 6, the STJ and POLJ do not appear to influence one another systematically, there are still instances in which the waviness of the two jets can be phased so as to promote intense interactions. Daily perusal of hemispheric synoptic maps suggests that such instances of jet interaction often lead to intense lower tropospheric cyclogenesis events. Current research is examining whether such jet interaction-induced cyclogenesis events from specific seasons systematically correspond to episodes of polar vortex weakening.

COMPETING INTERESTS: The contact author has declared that none of the authors has any competing interests.

AUTHOR CONTRIBUTIONS: J. Martin completed the ALD analysis and did all the writing, figure drafting and preparation of the manuscript for submission. T. Norton performed the analysis that determined the POLJ and STJ isentropic housings during SH winter.

ACKNOWLEDGEMENTS: This work was supported by the National Science Foundation under grants ATM-1640055 and NSF-2055667. JRA-55 data available from the Research Data Archive at the National Center for Atmospheric Research. The authors would like to thank Prof. Andrea A. Lopez-Lang for helpful comments and suggestions.

REFERENCES

Archer, C. L., and K. Caldeira, 2008: Historical trends in the jet stream. *Geo. Res. Let.*, **35**(8).

Bals-Elsholz, T. M., E. H. Atallah, L. F. Bosart, T. A. Wasula, M. J. Cempa, and A. R. Lupo, 2001: The wintertime Southern Hemisphere split jet: Structure, variability, and evolution. *J. Climate*, 14, 4191-4215.

Barnes, E. A., 2013: Revisiting the evidence linking Arctic amplification to extreme weather in midlatitudes. *Geophys. Res. Let.*, **40**, 4734-4739.

_____, and L. Polvani, 2013: Response of the midlatitude jets, and of their variability, to increased greenhouse gases in the CMIP5 models. *J. Climate*, 26, 7117-7135.

_____, and J. A. Screen, 2015: The impact of Arctic warming on the midlatitude jet-stream: Can it? Has it? Will it? *WIREs Clim Change*, **6**, 277–286. doi: 10.1002/wcc.337.

Blackport, R., and J. A. Screen, 2020: Insignificant effect of Arctic amplification on the amplitude of midlatitude atmospheric waves. *Science advances*, *6*(8), p.eaay2880.

Campitelli, E., L. B. Diaz, and C. Vera, 2021: Assessment of zonally symmetric and asymmetric components of the Southern Annular Mode using a novel approach. *Clim. Dyn.*, **58**, 161-178.

Chenoli, S. N., M. Y. Ahmad Mazuki, J. Turner, & A. A. Samah, 2017: Historical and projected changes in the Southern Hemisphere sub-tropical Jet during winter from the CMIP5 models. *Clim. Dyn.*, **48,** 661-681.

Christenson, C. E., J. E. Martin, and Z. J. Handlos, 2017: A synoptic-climatology of Northern Hemisphere, cold season polar and subtropical jet superposition events. *J. Climate*, **30**, 7231-7246.

Copernicus Climate Change Service (C3S) (2017): ERA5: Fifth generation of ECMWF atmospheric reanalyses of the global climate. Copernicus Climate Change Service Climate Data Store (CDS), *March 2020,* https://cds.climate.copernicus.eu/cdsapp#!/home

Cunningham, P., and D. Keyser, 2004: Dynamics of jet streaks in a stratified quasi-geostrophic atmosphere: Steady-state representations. *Quart. J. Roy. Meteor. Soc.,* **130,** 1579-1609.

desJardins, M. L., K. F. Brill, and S. S. Schotz, 1991: GEMPAK 5 Part I—GEMPAK 5 programmer's guide. National Aeronautics and Space Administration. [Available from Scientific and Technical Information Division, Goddard Space Flight Center, Greenbelt, MD 20771.].

DiCapua G., and D. Coumou,2016: Changes in the meandering of the Northern Hemisphere circulation. *Environ. Res. Lett*., **11**, 094028, doi:10.1088/1748-9326/11/9/094028.

Fan, K.: Zonal asymmetry of the Antarctic Oscillation. *Geophys. Res. Lett*., https://doi.org/10.1029/2006GL028045.

Fogt, R. L., J. M. Jones, and J. Renwick, 2012: Seasonal zonal asymmetries in the Southern Annular Mode and their impact on regional temperature anomalies. *J. Climate*, **25**, 6253-6270.

Fogt, R. L. and G. J. Marshall, 2020: The Southern Annular Mode: Variability, trends, and climate impacts across the Southern Hemisphere. *WIREs Climate Change*, **11(4)**:e652. https://doi.org/10.1002/wcc.652.

Francis, J. A., 2017: Why are Arctic linkages to extreme weather still up in the air?. *Bull. Amer. Meteor. Soc.,* **98**, 2551-2557.

_____, and S. J. Vavrus, 2012: Evidence linking Arctic amplification to extreme weather in mid-latitudes. *Geophys. Res. Let*., **39**, L06801, doi:10.1029/2012GL051000.

_____, and _____, 2015: Evidence for a wavier jet stream in response to rapid Arctic warming. *Environ. Res. Lett*. **10**, 014005, doi:10.1088/1748-9326/10/1/014005.

______, N, Skific, and S. J. Vavrus, 2018: North American weather regimes are becoming more persistent: Is Arctic amplification a factor? *Geophys Res.Lett*., https://doi.org/10.1029/2018GL080252.

Gallego, D., P. Ribera, R. Garcia-Herrera, E. Hernandez, and L. Gimeno, 2005: A new look for the Southern Hemisphere jet stream. *Climate Dyn*., **24**, 607-621.

Gillett, Z. E., H. H. Hendon, J. M. Arblaster, and E.-P. Lim, 2021: Tropical and extratropical influences on the variability of the Southern Hemisphere wintertime subtropical jet. *J. Climate*, **34**, 4009-4022.

Gong, D., and S. Wang, 1999: Definition of Antarctic oscillation index. *Geophys. Res. Lett*., **26**, 459-462.

Goyal, R., M. Jucker, A. Sen Gupta, H. H. Hendon, and M. H. England, 2021: Zonal wave 3 pattern in the Southern Hemisphere generated by tropical convection. *Nat. Geosci*., **14**, 732-738.

____, _____, _____, and M. H. England, 2022: A new zonal wave-3 index for the Southern Hemisphere. *J. Climate*, **35**, 5137-5149.

Kalnay, E. and co-authors, 1996: The NCEP/NCAR 40-year reanalysis project. *Bull. Amer. Meteor. Soc*., **77**, 437-470.

Kistler, R. and co-authors, 2001: The NCEP-NCAR 50-Year reanalysis: Monthly means CD-ROM and documentation. *Bull. Amer. Meteor. Soc*., **82**, 247-267.

Kobayashi, S., Y. Ota, Y. Harada, A. Ebita, M. Moriya, H. Onoda, K. Onogi, H. Kamahori, C.

Kobayashi, H. Endo, K. Miyaoka, and K. Takahashi, 2015: The JRA-55 reanalysis: General specifications and basic characteristics. *J. Meteor. Soc. Japan*, **93**, 5-48.

Koch, P., H. Wernli, and H. C. Davies, 2006: An event-based jet-stream climatology and typology. *Int. J. Climatology*, **26**, 283-301.

Limpasuvan, V., and D. L. Hartmann, 1999: Eddies and the annular modes of climate variability. *Geophys. Res. Lett.*, **26**, 3133–3136.

Lorenz, D. J., and E. T. DeWeaver, 2007: Tropopause height and zonal wind response to global warming in the IPCC scenario integrations. *J. Geophys. Res: Atmos*., **112**(D10).

Maher, P., M. E. Kelleher, P. G. Sansom, and J. Methven, 2020: Is the subtropical jet shifting poleward?. *Clim. Dyn.*, **54**, 1741-1759.

Manney, G.L., M. I. Hegglin, Z. D. Lawrence, K. Wargan, L. F. Millán, M. J. Schwartz, M. L. Santee, A. Lambert, S. Pawson, B. W. Knosp, and R. A. Fuller, 2017: Reanalysis comparisons of upper tropospheric–lower stratospheric jets and multiple tropopauses. *Atmos. Chem. and Phys.*, **17**, 11541-11566.

Manney, G. L., and M. I. Hegglin, 2018: Seasonal and regional variations of long-term changes in upper-tropospheric jets from reanalyses. *J. Climate*, **31**, 423-448.

Martin, J. E., 2021: Recent trends in the waviness of the Northern Hemisphere wintertime polar and subtropical jets. *JGR Atmos*., https://doi.org/10.1029/2020JD033668.

Martineaux, P., G. Chen, and D. A. Burrows, 2017: Wave events: Climatology, trends, and relationship to Northern Hemisphere blocking and weather extremes. *J. Climate*, **30**, 5675-5697.

Matsuno, T., 1971: A dynamical model of the stratospheric sudden warming. *J. Atmos. Sci., 2*8, 1479-1494.

Miller, R. L., G. A. Schmidt, and D. T. Shindell, 2006: Forced annular variations in the 20th century Intergovernmental Panel on Climate Change Fourth Assessment Report models. *J. Geophys. Res.*, **111**, D18101, doi:10.1029/2005JD006323.

Nakamura, H., and A. Shimpo, 2004: Seasonal variations in the Southern Hemisphere storm tracks and jet streams as revealed in a reanalysis data set. *J. Climate*, **17**, 1828-1844.

Peña-Ortiz, C., D. Gallego, P. Ribera, P. Ordonez, and M. D. C. Alvarez-Castro, 2013: Observed trends in the global jet stream characteristics during the second half of the 20th century, *J. Geophys. Res. Atmos*., **118,** 2702–2713, doi:10.1002/jgrd.50305.

Rosso, F. V., N. T. Boiaski, S. E. T. Ferraz, and T. C. Robles, 2018: Influence of the Antarctic oscillation on the South Atlantic convergence Zone. *Atmosphere*, *9*(11), 431.

Screen, J. A., and I Simmonds, 2013: Exploring links between Arctic amplification and mid-latitude weather. *Geophys. Res. Lett*., https://doi.10.1002/grl.50174.

Serreze, M.C., A. P. Barrett, J. C. Stroeve, D.N Kindig. and M.M. Holland, 2009: The emergence of surface-based Arctic amplification. *Cryosphere*, **3**, 11-19.

Silvestri, G., and C. Vera, 2009: Nonstationary impacts of the Southern Annular Mode on Southern Hemisphere climate. *J. Climate*, **22**, 6142–6148.

Spensberger, C., M. J. Reeder, T. Spengler, and M. Patterson, 2020: The connection between the Southern Annular Mode and a feature-based perspective on Southern Hemisphere midlatitude winter variability. *J. Climate*, **33**, 115,129.

Thompson, D., and J. Wallace, 2000: Annular modes in the extratropical circulation. Part I: Month-to-month variability. *J. Climate*., **13**, 1000-1016.

Vavrus, S. J., 2018: The influence of Arctic amplification on mid-latitude weather and climate. *Curr. Clim. Change. Rep*., **4**, 238-249.

_____, F. Wang, J. E. Martin, J. A. Francis, Y. Peings, and J. Cattiaux, 2017: Changes in North American circulation and extreme weather: Influence of arctic amplification and Northern Hemisphere snow cover. *J. Climate* , **30**, 4317-4333.

WMO. 2022. *Executive summary. Scientific assessment of ozone depletion: 2022, GAW report no. 278*. Geneva, Switzerland: WMO

Yin, J. H., 2005: A consistent poleward shift of the storm tracks in simulations of 21st century climate. *Geophys. Res. Let.*, **32**, L18701,doi:10.1029/2005GL023684.

	POLJ			***STJ***		
	NCEP	*JRA-55*	*ERA5*	*NCEP*	*JRA-55*	*ERA5*
1979	*-45.416403*	*-19.684881*	*-64.232707*	-3.7754167	11.1345645	0.70639878
1980	*-59.380403*	*-58.393881*	*-63.657707*	-3.2564167	4.47656452	-0.8576012
1981	18.8845972	36.4021194	21.8872927	-4.4154167	5.17956452	-2.2326012
1982	-24.813403	3.63785707	-15.198707	41.2785833	16.1355645	10.5773988
1983	-16.281403	35.8650731	-15.658707	*-18.131417*	*-10.037435*	*-21.992601*
1984	-14.954403	4.06711936	-6.9887073	15.8335833	19.8715645	11.5133988
1985	4.02659722	10.3371194	-20.535707	**54.3615833**	**38.7185645**	**21.4393988**
1986	24.2525972	43.6271194	20.5902927	-6.9904167	0.00256452	-10.285601
1987	62.9565972	77.0631194	16.8692927	-8.9194167	0.57256452	-9.2566012
1988	-2.5614028	-7.4278806	-35.518707	-1.9554167	2.34556452	-5.2936012
1989	-33.646403	9.93808658	-16.752707	35.2235833	29.6575645	19.4843988
1990	21.8045972	40.1761194	5.93129268	28.6225833	8.32356452	-0.0366012
1991	**98.1615972**	**104.846187**	**79.9922927**	15.9005833	13.6185645	10.0163988
1992	*-31.301403*	*-26.480881*	*-43.682707*	23.9145833	30.1255645	22.5733988
1993	45.9685972	64.4221194	23.6692927	-5.4784167	7.54756452	-0.9296012
1994	*-29.454403*	*-32.656881*	*-69.886707*	**51.5895833**	**30.9815645**	**21.4813988**
1995	-22.226403	-20.908881	-47.179707	*-5.1054167*	*-12.989435*	*-16.721601*
1996	**80.0555972**	**96.1361194**	**86.8222927**	-2.3444167	-10.092435	-11.395601
1997	**68.8895972**	**57.6655297**	**78.5282927**	2.23058333	-8.3644355	-11.693601
1998	*-27.166403*	*-32.68934*	*-70.988707*	18.5915833	-2.3754355	-7.9706012
1999	36.1115972	-22.593881	-44.562707	*3.60158333*	*-23.970435*	*-32.015601*
2000	57.1715972	17.3883325	16.0832927	49.9395833	18.8905645	12.2183988
2001	51.6315972	26.2991194	8.28429268	46.9905833	7.20656452	1.48939878
2002	30.0675972	35.9181194	21.4212927	**65.2545833**	**47.0115645**	**40.0813988**
2003	70.6935972	52.1291194	24.5692927	12.5915833	-3.7804355	-11.507601
2004	27.8395972	-18.835881	-31.660707	39.5535833	19.0855645	13.4163988
2005	48.0095972	26.0351194	-2.9987073	*-10.510417*	*-21.297435*	*-26.212601*
2006	76.9665972	27.7838267	24.9342927	29.3135833	-2.1904355	-10.139601
2007	60.9595972	55.4256292	46.9952927	38.6865833	17.2975645	14.1103988
2008	**67.6425972**	**67.2851194**	**66.7882927**	*-4.0874167*	*-21.790435*	*-25.102601*
2009	69.9215972	17.7955696	23.8622927	22.6285833	-4.6854355	-8.0676012
2010	41.5965972	13.4191194	3.93329268	31.9945833	16.0065645	11.1233988
2011	**118.932597**	**111.764119**	**79.1722927**	11.7745833	-5.6934355	-8.7496012
2012	38.3955972	9.84011936	-2.5287073	54.8005833	14.8235645	-1.2216012
2013	32.3355972	-0.7048806	-14.266707	**67.4165833**	**25.3645645**	**13.6133988**
2014	52.2325972	45.4011194	-60.736707	40.1415833	20.9895645	6.32532378
2015	65.0135972	38.0481194	18.8882927	14.6575833	1.69656452	-1.7356012
2016	51.9375972	19.3210046	15.3602927	22.3815833	2.71556452	-0.3676012
2017	15.4975972	-14.224881	-38.558707	30.2145833	2.97356452	-2.2008762
2018	70.8755972	21.0891194	3.86429268	3.15258333	-7.7994355	-11.277601
2019	68.5365972	5.97811936	-22.852707	**58.1465833**	**21.7315645**	**7.09439878**

TABLE 1 Integrated seasonal departures from average ALD (degrees) for polar and subtropical jets from the three reanalysis data sets employed in this work. Bold (underlined italics) represents one of the top 5 waviest (least wavy) seasons.

FIGURE CAPTIONS

Fig. 1 (a) Distribution of grid-column maximum wind speeds found in 5K isentropic layers from 10 - 80°S for every 6h analysis time in JJA from 1958-2019 from the JRA-55 reanalysis. (b) As for Fig. 1a except limited to (i) grid-columns in which the integral average wind speed from 400 to 100 hPa exceeded 30 m s^{-1} and (ii) to latitudes 0 - 40°S for the STJ and (iii) latitudes 40 to 65°S for the POLJ.

Fig. 2 (a) Isotachs of the daily averaged wind speed (contoured every 10 m s^{-1} and shaded above 30 m s^{-1}) and the core isertel (bold black line) in the 310:325K isentropic layer on 13 July 1995 from the JRA-55 reanalysis data. The core isertel value is -1.3 PVU. (b) As in (a) but for 24 August 2001. Core isertel value is -2.0 PVU. Dashed red line indicates portion of the core isertel from the overlying STJ layer (depicted in Fig. 2d). (c) As in (a) but for wind speeds and core isertel in the 340:355K isentropic layer on 13 July 1995. Core isertel value is -3.6 PVU. (d) As in (c) but for 24 August 2001. Core isertel value is -1.4 PVU. Dashed blue line indicates a portion of the core isertel from the underlying POLJ layer (depicted in Fig. 2b). See text for further explanation.

Fig. 3 (a) Solid (dashed) lines are the positions of the average core isertels of the STJ (POLJ) from each of the three reanalyses employed in this study. The different reanalyses are color coded. (b) Thick solid lines are the positions of the average core isertels for the STJ from each of the reanalyses superimposed with JJA average 200 hPa isotachs from the NCEP-NCAR reanalysis. (c) Thick dashed lines are the positions of the average core isertels for the POLJ superimposed with JJA average 700 hPa isotachs from the NCEP-NCAR reanalysis.

Fig. 4 Frequency of occurrence of the core isertel value for each reanalysis time series in (a) the STJ layer and (b) the POLJ layer. Solid blue, red and green lines in (a) and (b) are the SH distributions from the NCEP, JRA55 and ERA5, respectively. The dashed blue, red and green lines are the NH distributions from the NCEP, JRA55 and ERA5 reanalyses, respectively. In (b), the NH distributions are from the 315:330K layer which houses the POLJ in the boreal winter. Thin blue, red and green lines in (a) and (b) indicate the peak values of the core isertel in each layer from each data set. Isertel values are given in potential vorticity units (PVU, 1 PVU = 10^{6} K m^{2} kg^{-1} s^{-1}), and are multiplied by -1 for the NH values.

Fig. 5 Seasonal average ALD (in degrees) of the SH wintertime subtropical and polar jets for each cold season in the three reanalysis time series. The polar jet values are in the three shades of blue while the subtropical jet values are in the three three shades of red. The dashed black line through each time series represents the trend line for each (derived from the JRA-55 time series) and is significant at the 96% level. Gray lines are the boreal winter ALD analysis from Fig. 6 of Martin (2021).The "YEAR" on the abscissa indicates the year in which December of that cold season occurred.

Fig. 6 Time series of the daily ALD of the polar (blue lines) and subtropical (red lines) jets from the (a) NCEP-Reanalysis, (b) JRA-55, and (c) ERA5 data sets for austral winter 1999. The correlation between the two times series from each data set is indicated.

Fig. 7 Seasonal average **U** along the core isertel for the subtropical (red lines) and polar (blue lines) jets from each of the three SH reanalysis data sets. The thin black lines are trend lines for each time series from the JRA-55 data. Gray lines are the equivalent boreal winter **U** analysis from Fig. 9 of Martin (2021).

Fig. 8 Time series of the seasonal average equivalent latitude of the polar (blue lines) and subtropical (red lines) jets from the three different SH reanalysis data sets. The thin black lines are the trend lines (from the JRA-55 data) and are significant above the 99% leve for both jet species. Gray lines are the boreal winter equivalent latitude analysis from Fig. 10 of Martin (2021).

Fig. 9 JJA average SAM index (histogram) from NCEP's Climate Prediction Center. The index is calculated by projecting the daily 700 hPa geopotential height anomalies poleward of 20S onto the leading pattern of the Antarctic Oscillation (AAO) ofGong and Wang (1999). Black solid line is theJJA average ALD of the POLJ from the JRA-55 reanalysis.

Fig. 10 Spaghetti plots of core isertels from SH summer months with maximum positive (red) and negative (blue) SAM indices since 1979. (a) Daily JRA-55 core isertels from June 2009, the June with the most positive SAM in the record. (b) As for Fig. 10a but for June 1992, the June with the most negative SAM in the record. (c) As for Fig. 10a but for July 1998. (d) As for Fig. 10b but for July 1995. (e) As for Fig. 10a but for August 1994. (f) As for Fig. 10b but for August 1981. Average ALD for the given months are listed in the bottom left of each panel.

Fig. 11 500 hPa height differences between the composite waviest and least wavy (a) polar jet and (b) subtropical jet seasons constructed from the JRA-55 reanalysis. See Table 1 for identification of the specific years comprising each composite. Positive (negative) height differences are in solid red (blue) lines labeled in m and contoured every 10 m (-10 m) beginning at 10 m (-10 m).

Fig. 12 250 hPa height differences between the composite waviest and least wavy (a) polar jet and (b) subtropical jet seasons constructed from the JRA-55 reanalysis. See Table 1 for identification of the specific years comprising each composite. Positive (negative) height differences are in solid red (blue) lines labeled in m and contoured every 10 m (-10 m) beginning at 10 m (-10 m).

Fig. 13 50 hPa height differences between the composite waviest and least wavy (a) polar jet and (b) subtropical jet seasons constructed from the JRA-55 reanalysis. See Table 1 for identification of the specific years comprising each composite. Positive (negative) height differences are in solid red (blue) lines labeled in m and contoured every 10 m (-10 m) beginning at 10 m (-10 m).

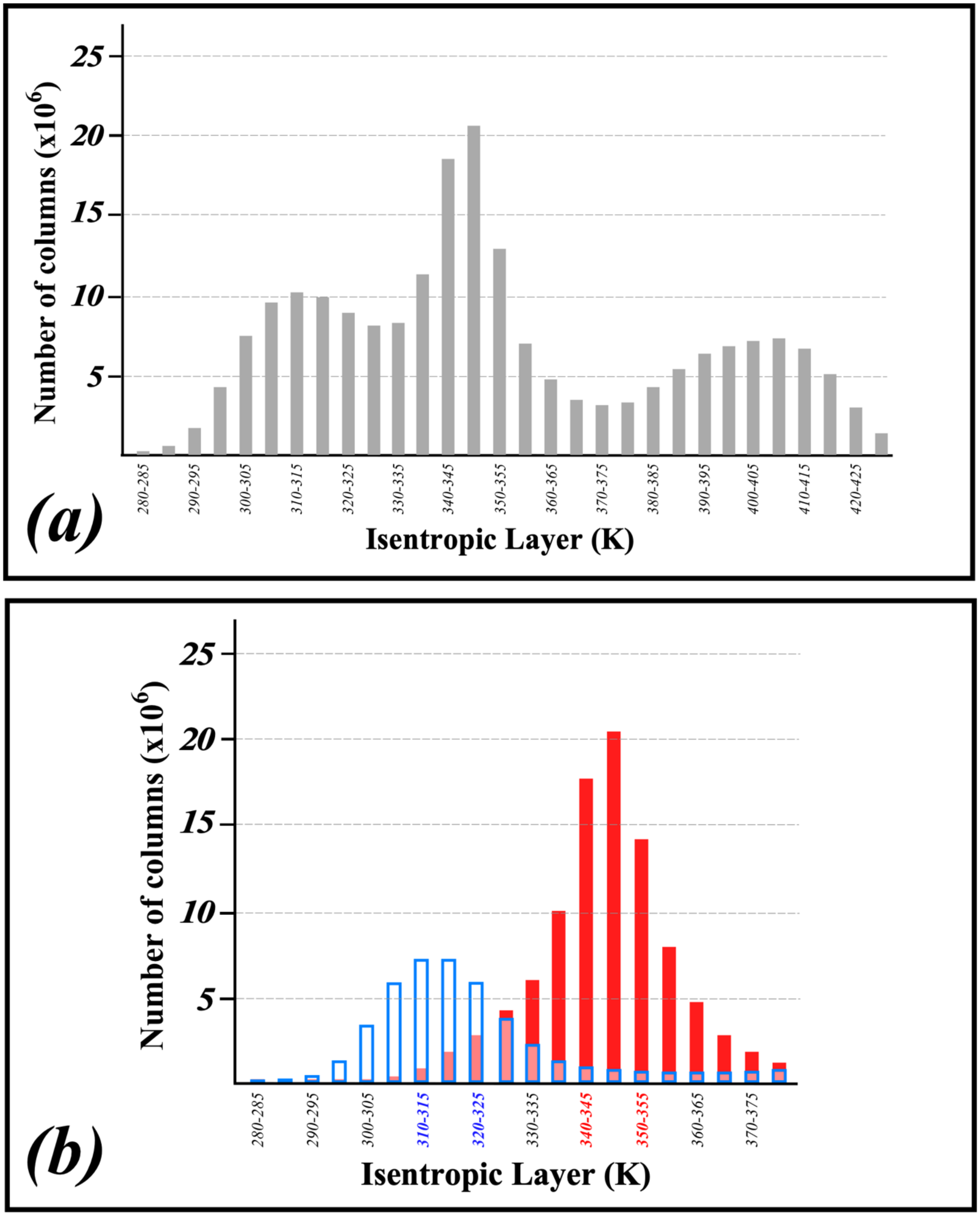

Fig. 1 (a) Distribution of grid-column maximum wind speeds found in 5K isentropic layers from 10 - 80°S for every 6h analysis time in JJA from 1958-2019 from the JRA-55 reanalysis. (b) As for Fig. 1a except limited to (i) grid-columns in which the integral average wind speed from 400 to 100 hPa exceeded 30 m s^{-1} and (ii) to latitudes 0 - 40°S for the STJ and (iii) latitudes 40 to 65°S for the POLJ.

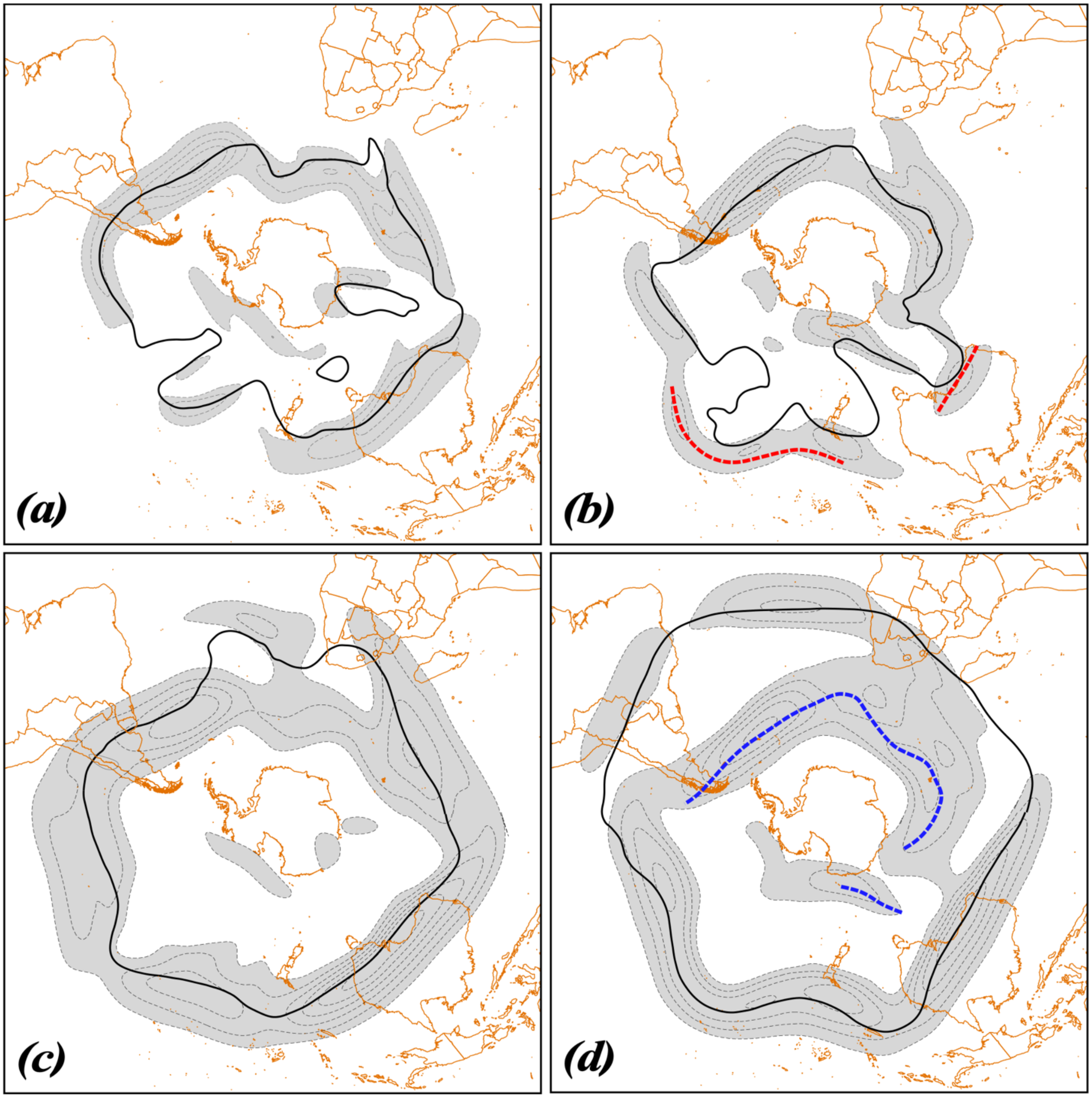

Fig. 2 (a) Isotachs of the daily averaged wind speed (contoured every 10 ma-1 and shaded above 30 m s-1) and the core isertel (bold black line) in the 310:325K isentropic layer on 13 July 1995 from the JRA-55 reanalysis data. The core isertel value is -1.3 PVU. (b) As in (a) but for 24 August 2001. Core isertel value is -2.0 PVU. Dashed red line indicates portion of the core isertel from the overlying STJ layer (depicted in Fig. 2d). (c) As in (a) but for wind speeds and core isertel in the 340:355K isentropic layer on 13 July 1995. Core isertel value is -3.6 PVU. (d) As in (c) but for 24 August 2001. Core isertel value is -1.4 PVU. Dashed blue line indicates a portion of the core isertel from the underlying POLJ layer (depicted in Fig. 2b). See text for further explanation.

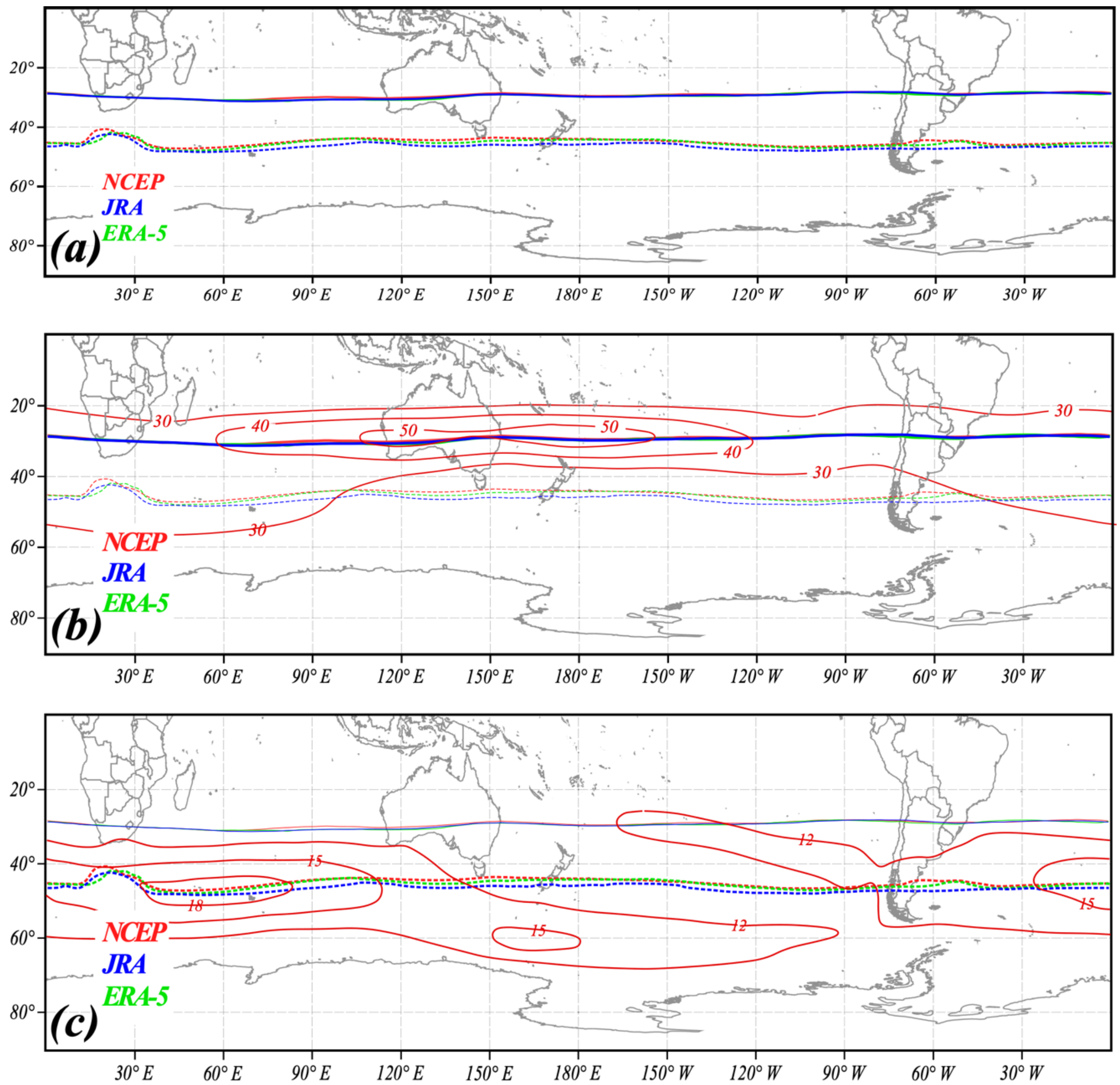

Fig. 3 (a) Solid (dashed) lines are the positions of the average core isertels of the STJ (POLJ) from each of the three reanalyses employed in this study. The different reanalyses are color coded. (b) Thick solid lines are the positions of the average core isertels for the STJ from each of the reanalyses superimposed with JJA average 200 hPa isotachs from the NCEP-NCAR reanalysis. (c) Thick dashed llines are the positions of the average core isertels for the POLJ superimposed with JJA average 700 hPa isotachs from the NCEP-NCAR reanalysis.

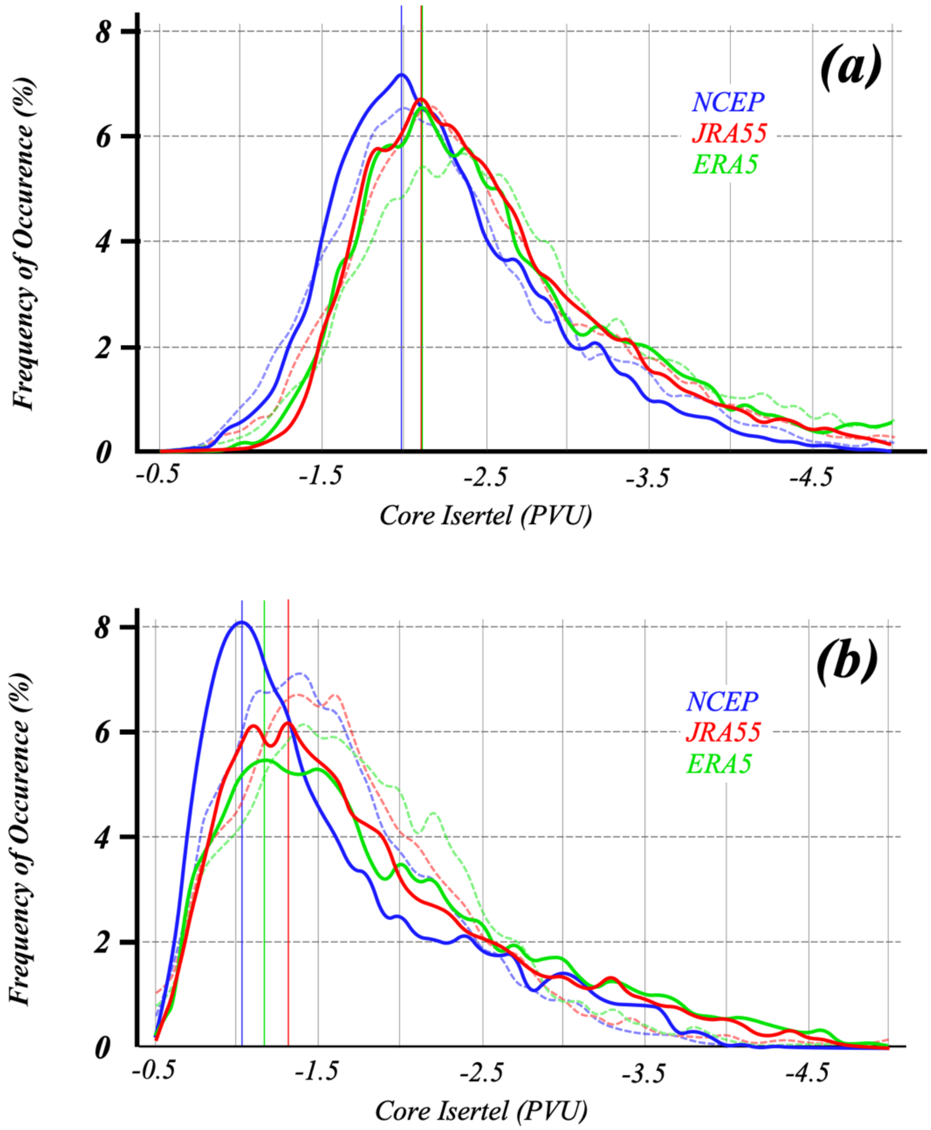

Fig. 4 Frequency of occurrence of the core isertel value for each reanalysis time series in (a) the STJ layer and (b) the POLJ layer. Solid blue, red and green lines in (a) and (b) are the SH distributions from the NCEP, JRA55 and ERA5, respectively. The dashed blue, red and green lines are the NH distributions from the NCEP, JRA55 and ERA5 reanalyses, respectively. In (b), the NH distributions are from the 315:330K layer which houses the POLJ in the boreal winter. Thin blue, red and green lines in (a) and (b) indicate the peak values of the core isertel in each layer from each data set. Isertel values are given in potential vorticity units (PVU, 1 PVU = 10^{6} K m^{2} kg^{-1} s^{-1}) and are multplied by -1 for the NH values.

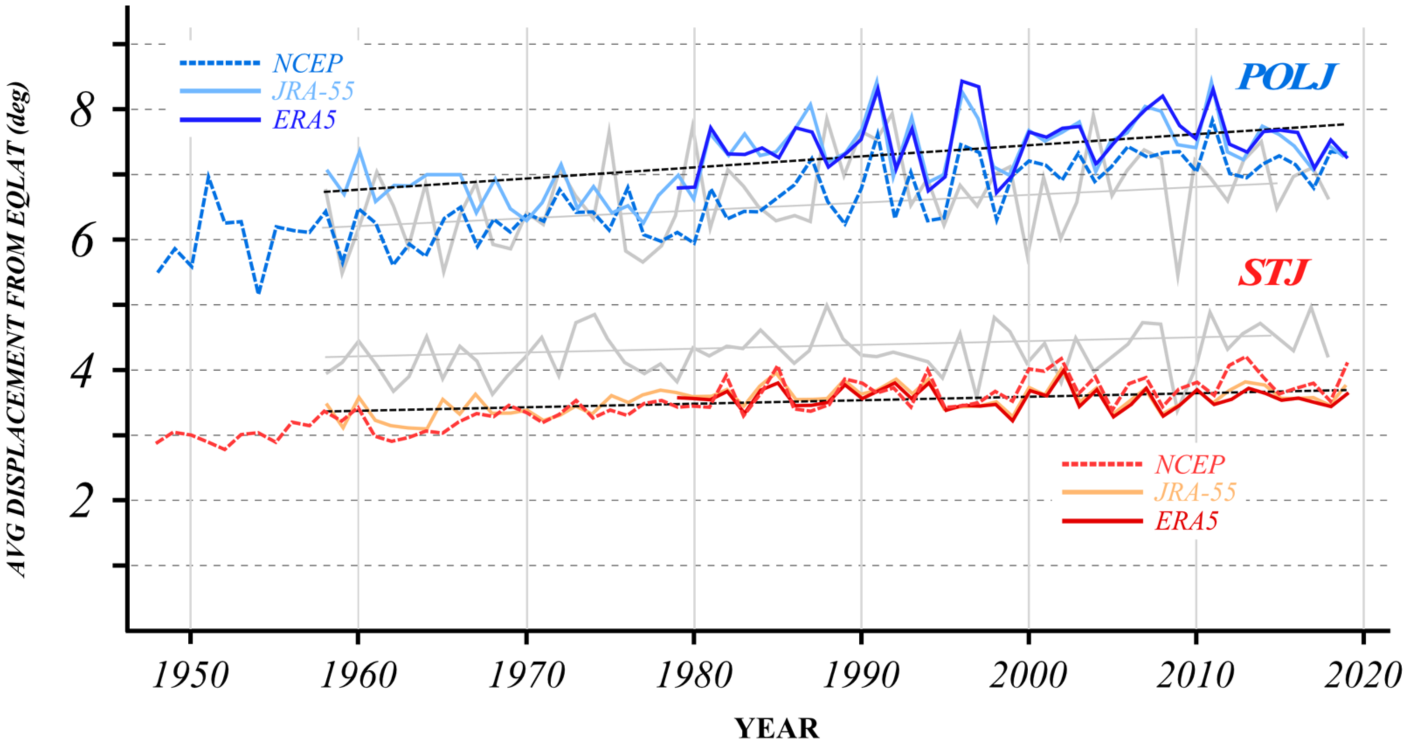

Fig. 5 Seasonal average ALD (in degrees) of the SH wintertime subtropical and polar jets for each cold season in the three reanalysis time series. The polar jet values are in the three shades of blue while the subtropical jet values are in the three three shades of red. The dashed black line through each time series represents the trend line for each (derived from the JRA-55 time series) and is significant at the 96% level. Gray line is the boreal winter average ALD from 1958 onward portrayed in Fig. 6 of Martin (2021).The "YEAR" on the abscissa indicates the year in which December of that cold season occurred.

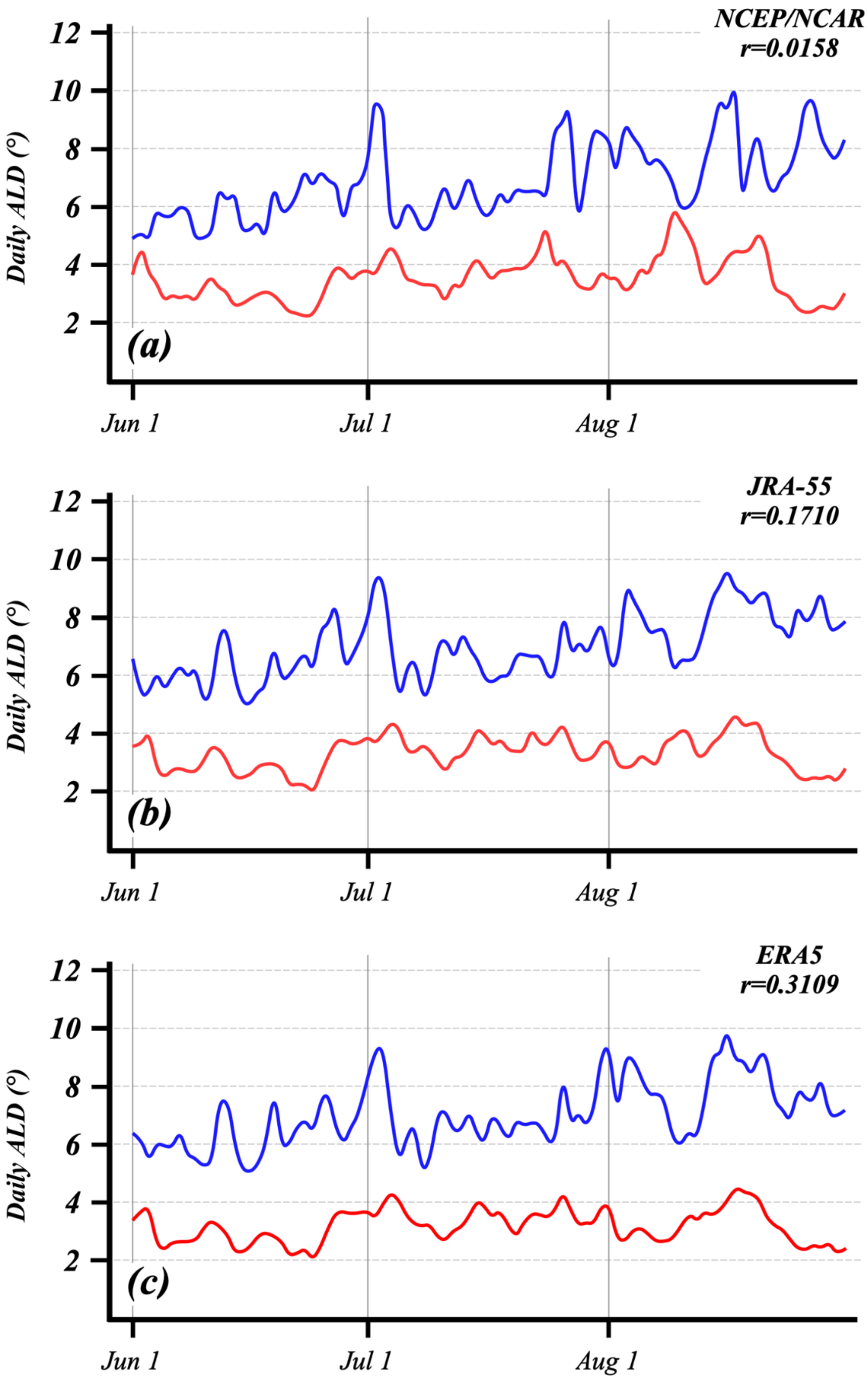

Fig. 6 Time series of the daily ALD of the polar (blue lines) and subtropical (red lines) jets from the (a) NCEP-Reanalysis, (b) JRA-55, and (c) ERA5 data sets for austral winter 1999. The correlation between the two times series from each data set is indicated.

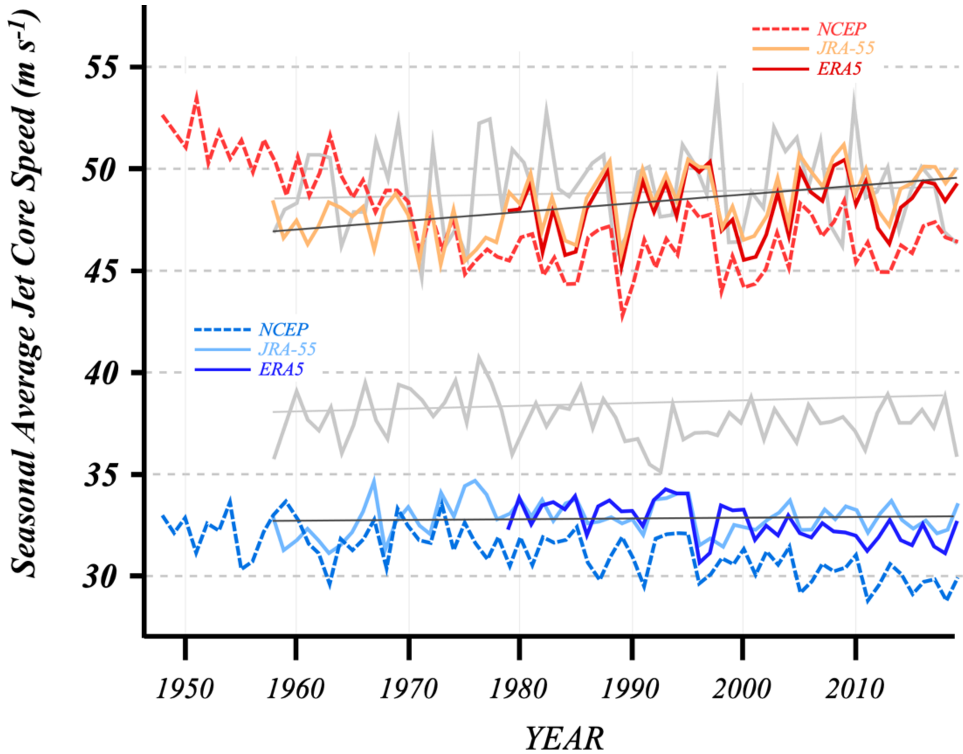

Fig. 7 Seasonal average **U** along the core isertel for the subtropical (red lines) and polar (blue lines) jets from each of the three SH reanalysis data sets. The thin black lines are trend lines for each time series from the JRA-55 data. Gray line is the average (1958-2018) boreal winter **U** analysis for each jet from the three data sets in Fig. 9 of Martin (2021).

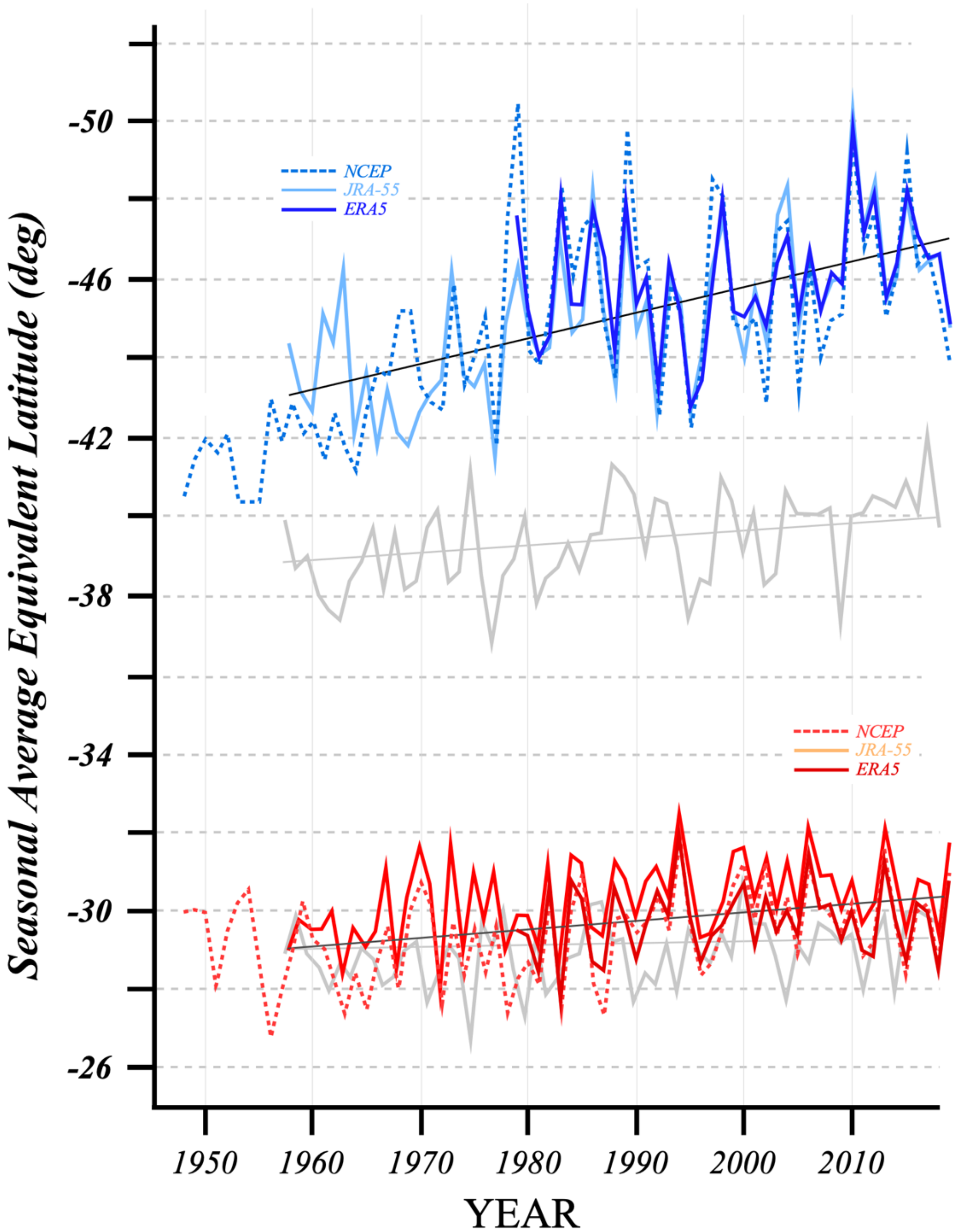

Fig. 8 Time series of the seasonal average equivalent latitude of the polar (blue lines) and subtropical (red lines) jets from the three different SH reanalysis data sets. The thin black lines are the trend lines (from the JRA-55 data) and are significant abov e the 99% level for both jet species. Gray line is the boreal winter average (1958-2017) equivalent latitude for each jet from the three reanalysis data sets portrayed in Fig. 10 of Martin (2021).

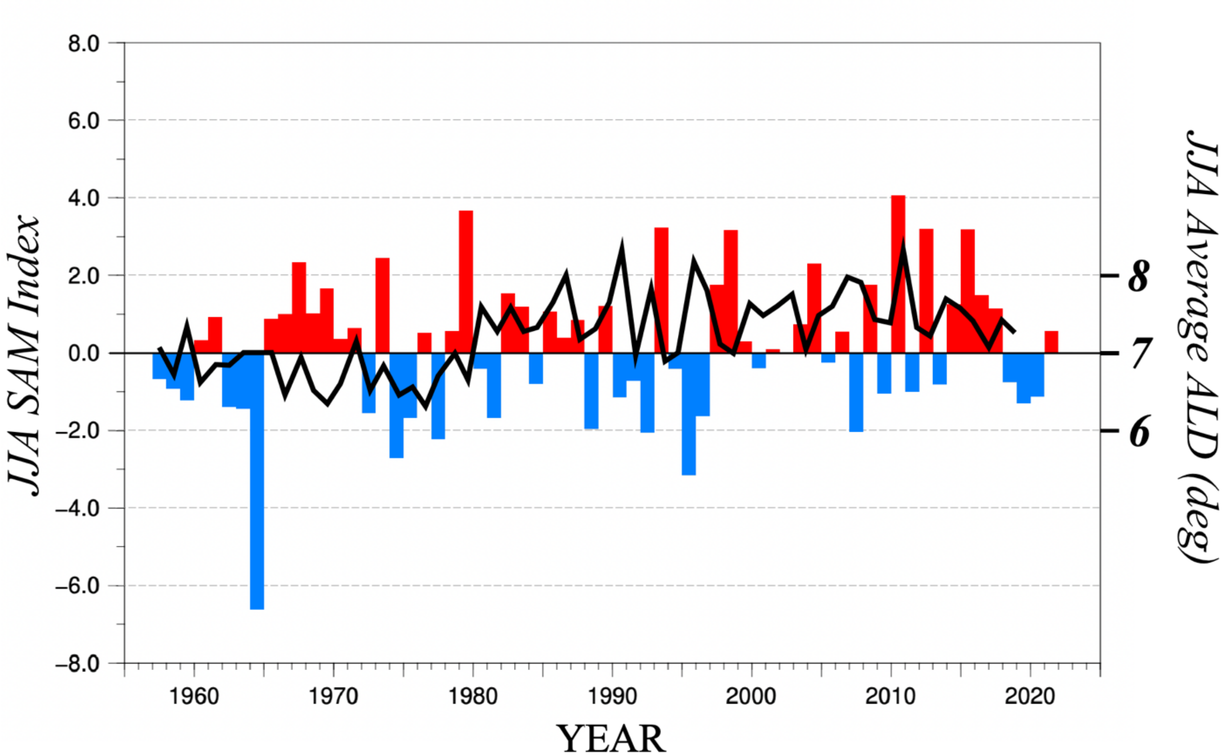

Fig. 9 JJA average SAM index (histogram) from NCEP's Climate Prediction Center. The index is calculated by projecting the daily 700 hPa geopotential height anomalies poleward of 20S onto the leading pattern of the Antarctic Oscillation (AAO) ofGong and Wang (1999). Black solid line is the JJA average ALD of the POLJ from the JRA-55 reanalysis.

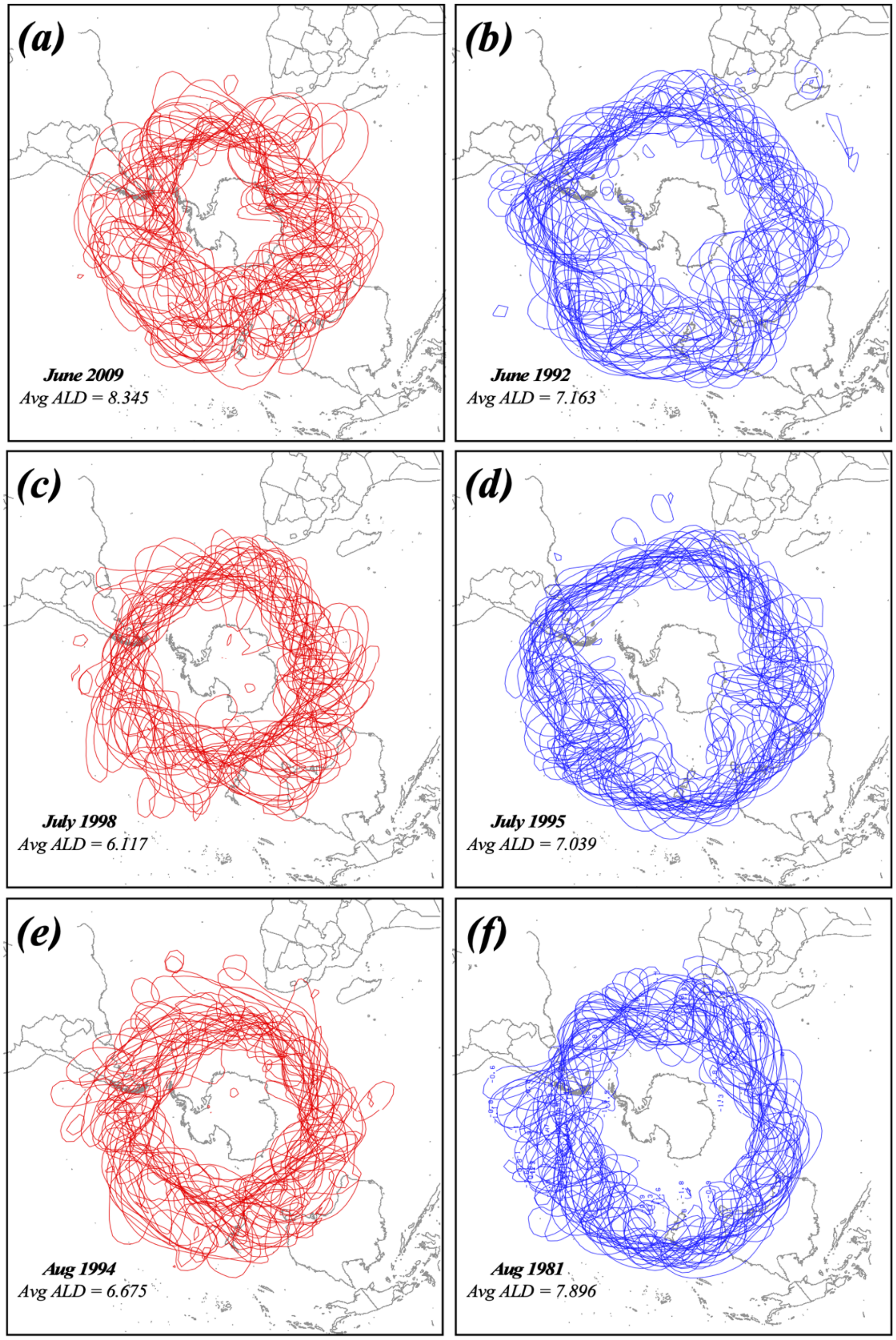

Fig. 10 Spaghetti plots of core isertels from SH summer months with maximum positive (red) and negative (blue) SAM indices since 1979. (a) Daily JRA-55 core isertels from June 2009, the June with the most postive SAM in the record. (b) As for Fig. 10a but for June 1992, the June with themost negative SAM in the record. (c) As for Fig. 10a but for July 1998. (d) As for Fig. 10b but for July 1995. (e) As for Fig. 10a but for August 1994.(f) As for Fig. 10b but for August 1981. Average ALD for the given months are listed in the bottom left of each panel.

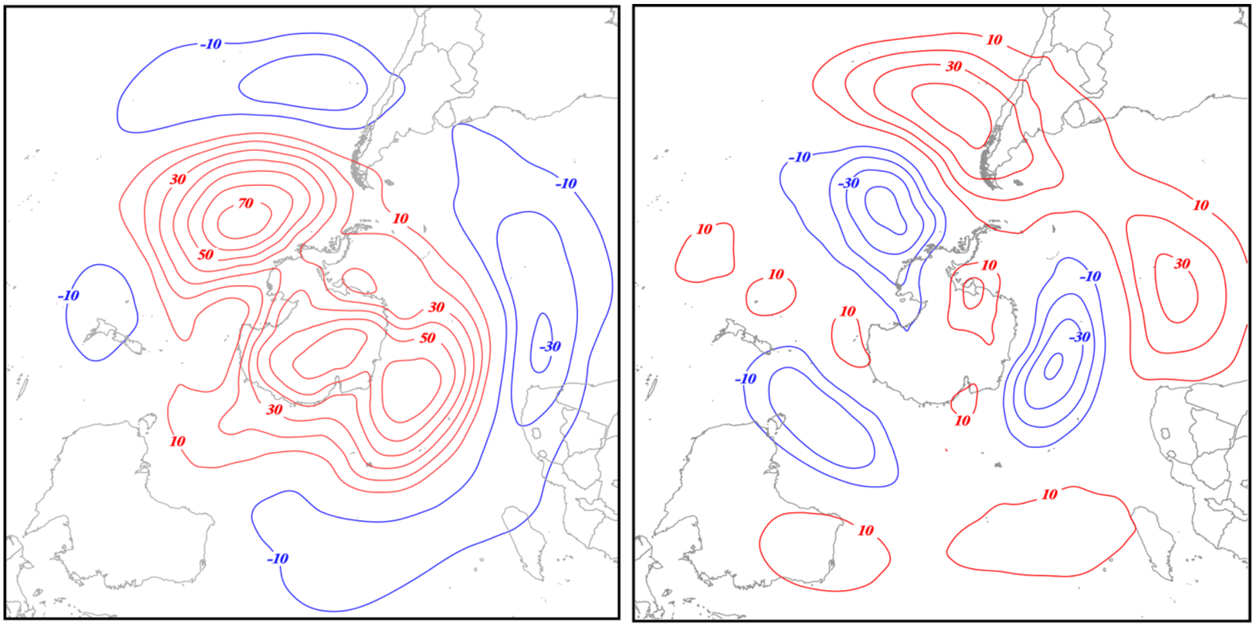

Fig. 11 500 hPa height differences between the composite waviest and least wavy (a) polar jet and (b) subtropical jet seasons constructed from the JRA-55 reanalysis. See Table 1 for identification of the specific years comprising each composite. Positive (negative) height differences are in solid red (blue) lines labeled in m and contoured every 10 m (-10 m) beginning at 10 m (-10 m).

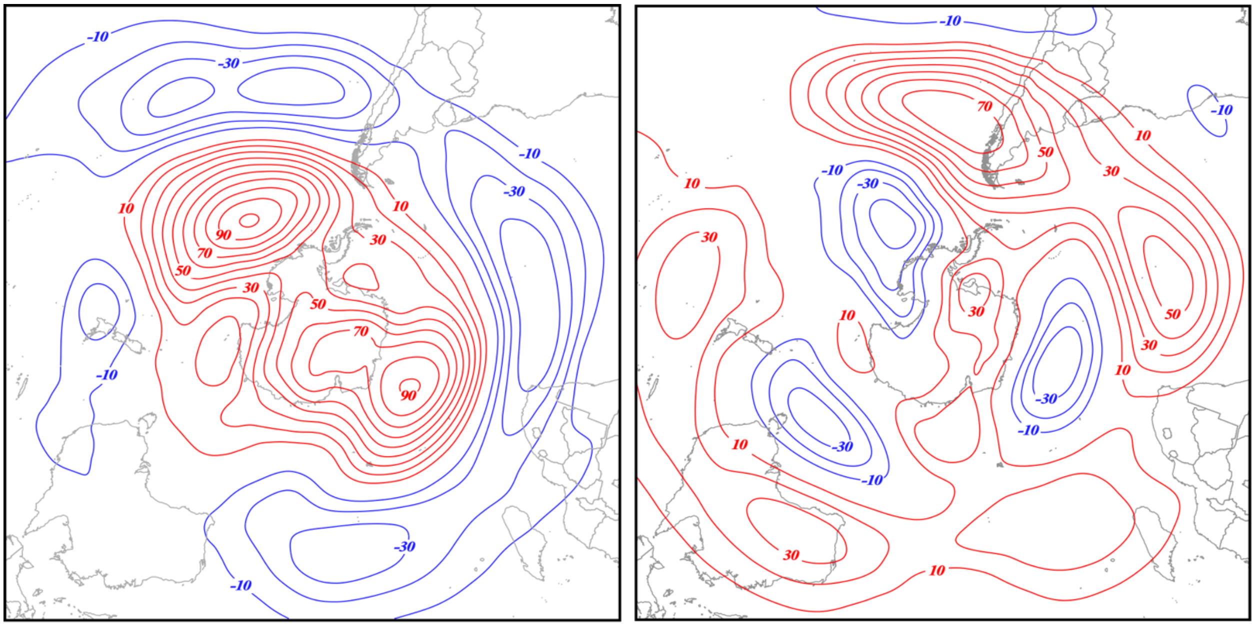

Fig. 12 250 hPa height differences between the composite waviest and least wavy (a) polar jet and (b) subtropical jet seasons constructed from the JRA-55 reanalysis. See Table 1 for identification of the specific years comprising each composite. Positive (negative) height differences are in solid red (blue) lines labeled in m and contoured every 10 m (-10 m) beginning at 10 m (-10 m).

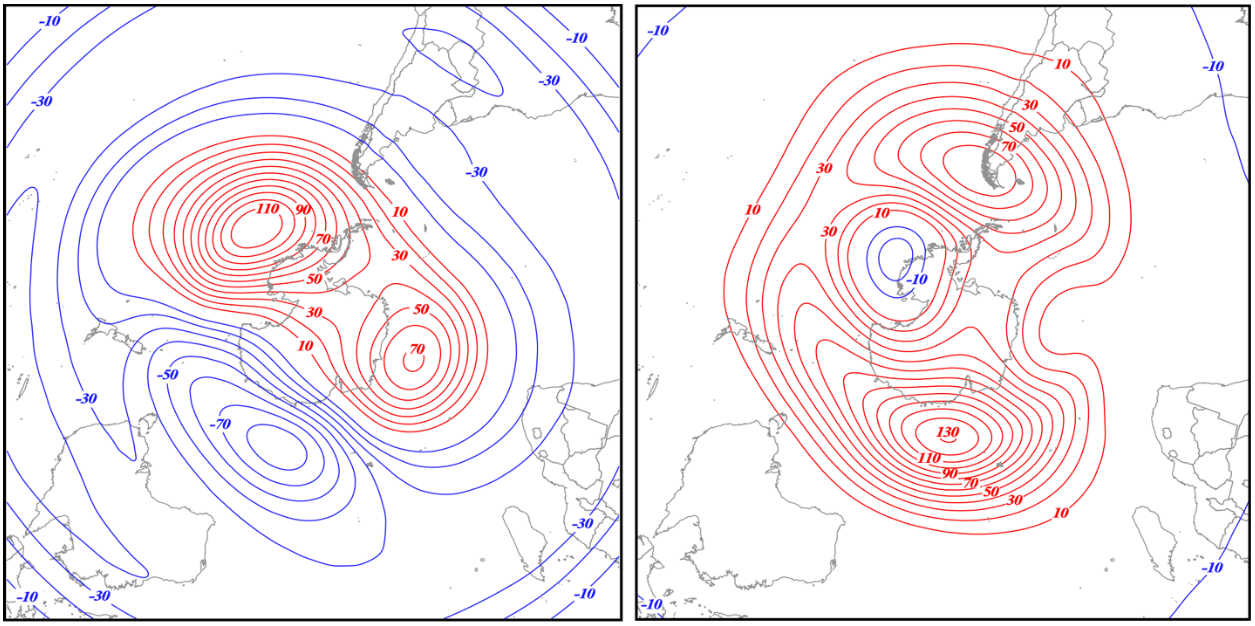

Fig. 13 50 hPa height differences between the composite waviest and least wavy (a) polar jet and (b) subtropical jet seasons constructed from the JRA-55 reanalysis. See Table 1 for identification of the specific years comprising each composite. Positive (negative) height differences are in solid red (blue) lines labeled in m and contoured every 10 m (-10 m) beginning at 10 m (-10 m).